ACS APPLIED MATERIALS & INTERFACES

Research Article

www.acsami.org

Nafion-Modified MoO_x as Effective Room-Temperature Hole Injection Layer for Stable, High-Performance Inverted Organic Solar Cells

Weiming Qiu,*[,†,‡] Robert Müller,[†] Eszter Voroshazi,[†] Bert Conings,[∥] Robert Carleer,[∥] Hans-Gerd Boyen,[∥] Mathieu Turbiez,[⊥] Ludo Froyen,[‡] Paul Heremans,[†,§] and Afshin Hadipour[†]

[†]Imec, Kapeldreef 75, 3001 Heverlee, Belgium

[‡]Department of Metallurgy and Materials Engineering and [§]Department of Electrical Engineering (ESAT), KU Leuven, 3001 Heverlee, Belgium

[∥]Institute for Materials Research, University of Hasselt, Wetenschapspark 1, 3590 Diepenbeek, Belgium

[⊥]BASF Schweiz AG, Schwarzwaldallee 215, CH-4002 Basel, Switzerland

Supporting Information

ABSTRACT: We present a hole injection layer processed from solution at room temperature for inverted organic solar cells. Bis(2,4-pentanedionato) molybdenum(VI) dioxide ($MoO_2(acac)_2$) is used as the precursor for MoO_x. Small amounts of Nafion in the precursor solution allow it to form continuous films with good wetting onto the active layers. The hydrolysis of $MoO_2(acac)_2$ and the effects of adding Nafion to the precursor solution are studied by Fourier transform infrared spectroscopy and X-ray photoelectron spectroscopy. The devices with solution-processed MoO_x including Nafion exhibited comparable performance to the reference devices based on the commonly used hole injection layers such as poly(3,4-ethylenedioxythiophene):polystyrenesulfonate (PEDOT:PSS) or evaporated MoO_3. Inverted poly(3-hexylthiophene):[6,6]-phenyl C61-butyric acid methyl ester devices with Nafion-modified MoO_x maintain 80% of their initial power conversion efficiency upon exposure to ambient air for ∼5000 h, outperforming devices with PEDOT:PSS or with evaporated MoO_3.

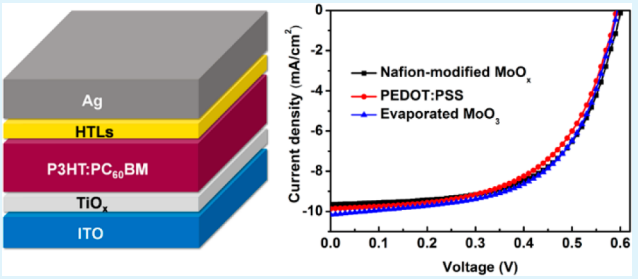

KEYWORDS: *Nafion, MoO_x, hole injection layer, inverted solar cells, stability*

1. INTRODUCTION

Organic solar cells have attracted large interest during the past decade as thin-film photovoltaic technology with the potential of delivering low-cost, semitransparent photovoltaic devices on a variety of substrates including flexible plastic films.[1−4] Recently, organic solar cell with power conversion efficiencies exceeding 10% have been shown with both polymers and small molecule materials,[5,6] which is a significant step toward the key 10−10 target (10% efficiency and 10 years of stability).[7] To further increase the efficiency and the stability, one of the crucial aspects is engineering of the interface between the electrodes and the active layers by using electron injection layers and hole injection layers (HILs).[8−11] Although poly(3,4-ethylenedioxythiophene):polystyrenesulfonate (PEDOT:PSS) has been widely used as HIL, by virtue of its good electrical properties and excellent solution processability, its acidic and hygroscopic nature are detrimental to the long-term stability of organic solar cells.[12−15] Therefore, the search for new hole buffer layer materials that can replace PEDOT:PSS is an important research area. Especially, solution-processed high work function transition metal oxides, such as MoO_3,[16−22] V_2O_5,[23−29] NiO,[30−33] and WO_3,[34−37] have been widely investigated and considered as promising alternatives to PEDOT:PSS, due to their favorable band structures, excellent stability in the ambient environment, and compatibility with large-area solution processing technologies. Devices with such metal oxide HILs have been reported to show comparable efficiency but increased stability over the ones using PEDOT:PSS.[21,27,32,33]

Most of the above-mentioned solution-processed metal oxide HILs, however, are only suitable for organic solar cells based on the conventional structure, where the HIL is deposited directly on indium tin oxide (ITO) covered glass substrates. Examples of HILs in high-performance inverted devices, where the HIL is deposited onto active layers, remain very scarce.[29,34,37−39] So far, thermally evaporated metal oxide HILs are still dominant in inverted devices. The reasons for the unsuccessful application of solution-processed metal oxide HILs in inverted device structures can be summarized as follows. First, sol−gel methods have been extensively used to make transition metal oxide based HILs. However, the temperature needed to convert the precursors into metal oxide is typically incompatible with the

Received: October 27, 2014
Accepted: January 28, 2015
Published: January 28, 2015

DOI: 10.1021/am507459t
ACS Appl. Mater. Interfaces 2015, 7, 3581−3589

organic active layers.[16,33] Furthermore, the hydrophobic nature of the active layer can cause dewetting issues during the processing of the metal oxide HILs, especially for water-based solutions. While the surface properties of ITO substrates can be easily tuned by O_2 plasma or UV−ozone to improve wetting, such treatments are harmful to the active layers. Finally, some highly reactive precursors for transition metal oxides can penetrate into the active layer and react with the active materials.[28,29] For example, Riedl and co-workers reported that vanadium(V) oxytriisopropoxide, a commonly used precursor for sol−gel V_2O_5, could diffuse deeply inside the active layer, degrading the device performance.[29]

In general, it is believed that the stability of inverted organic solar cells outperforms the stability of the conventional structures: the low work function metal cathodes of the latter ones suffer from rapid oxidation.[12,40] Moreover, recent work by McGehee et al. suggested that inverted devices are thermally more stable than their conventional counterparts, where a thin polymer-rich electron blocking layer between the active layer and the electron-extracting electrode can form under heat stress.[41] Consequently, the inverted device architecture is favored in the manufacturing of stable organic photovoltaic devices. This justifies the importance of the search for low-temperature solution-processed stable HILs that are applicable on top of organic semiconductors in an inverted device geometry. In literature, examples of HILs made from alcohol dispersions of metal oxide nanoparticles,[34,37,42,43] graphene oxide (GO),[44] and MoS_2[45,46] have been demonstrated. These address some of the issues mentioned above, but they each come with their own challenges, such as the aggregation of the nanomaterials in solution, or the requirement of postdeposition treatments like UV−ozone and O_2−plasma to improve the quality of as-prepared HILs.[43,46]

$MoO_2(acac)_2$ is readily hydrolyzed in various alcohols in ambient or N_2 atmosphere, and thus, it has been investigated by different groups as a precursor to synthesize low-temperature (<150 °C) solution-processed MoO_x HILs for conventional organic photovoltaic devices.[21,22,47] However, as will be shown below, such solution-processed MoO_x cannot be applied to inverted devices because of the poor wetting on the active layer during spin-coating. In this work, we show that the wetting issue can be solved by modifying the MoO_x solution with Nafion, a commercially available perfluorinated sulfonic acid ionomer. By doing this, we were able to process Nafion-modified solution-processed MoO_x layers on top of different types of active layers, without further postdeposition treatment like thermal annealing. Inverted devices with this room-temperature solution-processed HIL have comparable performance to the ones based on the benchmark HILs, that is, evaporated MoO_3 or PEDOT:PSS. Moreover, inverted poly(3-hexylthiophene):[6,6]-phenyl C61-butyric acid methyl ester (P3HT:$PC_{60}BM$) devices with Nafion-modified MoO_x HILs maintain more than 80% of their initial power conversion efficiency (PCE) after storage in air for ∼5000 h, outperforming those using the benchmark HILs.

2. RESULTS AND DISCUSSION

The chemical structures of $MoO_2(acac)_2$ and Nafion are shown in Scheme 1. For the preparation of Nafion-modified MoO_x, both materials were first dissolved separately in a mixture of 2-propanol and 1-butanol and were then mixed together before usage. Although 2-propanol and 1-butanol demonstrate good wetting properties on organic active layers, direct spin-coating

Scheme 1. Chemical Structures of $MoO_2(acac)_2$ and Nafion

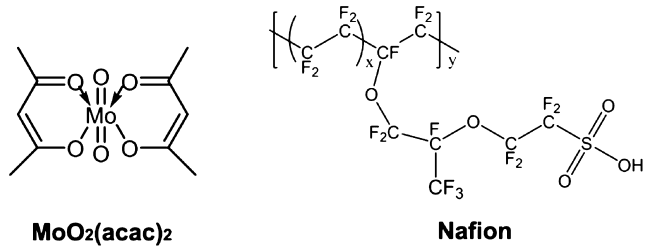

of a $MoO_2(acac)_2$ solution onto P3HT:$PC_{60}BM$ layers results in scattered islands instead of a continuous film (Figure 1a).

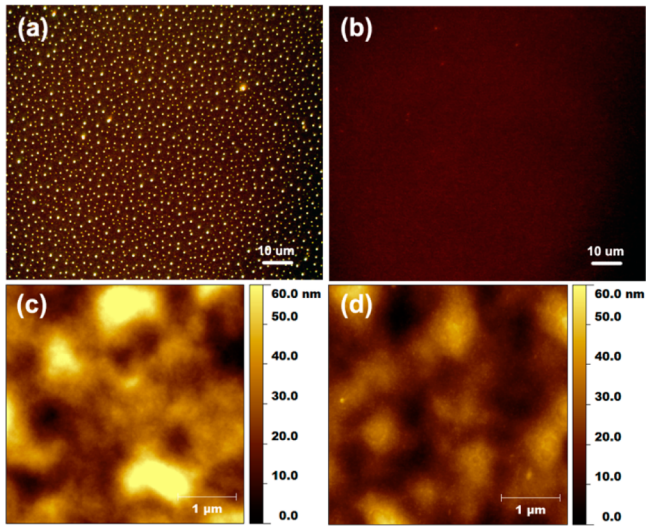

Figure 1. (a) Optical microscopy image of P3HT:$PC_{60}BM$ film after spin coating with $MoO_2(acac)_2$ solution. (b) Optical microscopy image of the P3HT:$PC_{60}BM$ film after spin coating with the mixed solution. (c) AFM image of P3HT:$PC_{60}BM$ film. (d) AFM image of P3HT:$PC_{60}BM$ film with Nafion-modified MoO_x on top.

This is probably due to the low viscosity of the solution and poor interaction between the solute and the active layer. Therefore, Nafion was chosen as additive to modify the $MoO_2(acac)_2$ solution. On one hand, Nafion can increase the viscosity of the solution owing to its polymeric nature; on the other hand, the polymer backbone and the $-SO_3^{2-}$ (or $-SO_3H$) end group of Nafion can favorably interact with the organic active layer and the polymolybdate species, respectively. As shown in Figure 1b, a smooth film was obtained from the mixture solution of $MoO_2(acac)_2$ and Nafion. Furthermore, atomic force microscopy (AFM) measurements indicate that the deposition of a Nafion-modified MoO_x layer on aP3HT:$PC_{60}BM$ blend slightly reduced the surface roughness (root-mean-square) from 12.64 to 8.34 nm (Figure 1c,d).

To understand the chemical evolution and the interaction between the precursors, Fourier transform infrared (FT-IR) and X-ray photoelectron spectroscopy (XPS) measurements were carried out for films deposited on KBr crystals and on silicon substrates, respectively. Figure 2 illustrates the FT-IR spectra of the films obtained from different solutions. All samples studied here have an absorption band at 1621 cm^{-1} and a broad band centered at 3490 cm^{-1} (not shown), which corresponds to the bending modes of adsorbed H_2O and the stretches associated with −OH, respectively.[22] For the film

DOI: 10.1021/am507459t
ACS Appl. Mater. Interfaces 2015, 7, 3581−3589

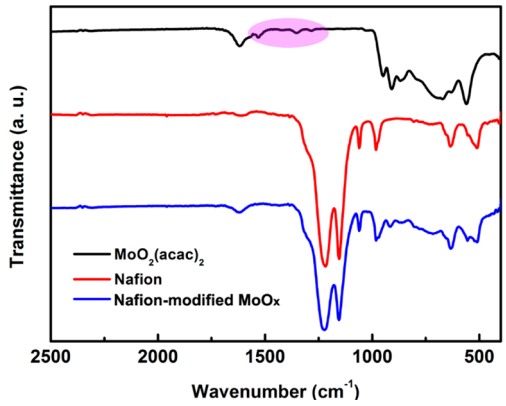

Figure 2. FT-IR spectra of the films spin coated from $MoO_2(acac)_2$, Nafion, and the mixed solutions, respectively. The typical absorption bands of acetylacetonate groups are marked in the purple area.

spin-coated from $MoO_2(acac)_2$ solution, the split band at 949 and 910 cm^{-1} is the characteristic of Mo═O bonds.[48] More importantly, compared to the spectra of $MoO_2(acac)_2$ powder (Supporting Information, Figure S1), a strong absorption band with multiple peaks centered at 700 cm^{-1} is observed; this can be assigned to Mo−O−Mo bonds.[22,49] The existence of such broad bands in the 900−500 cm^{-1} spectral region suggests the hydrolysis of $MoO_2(acac)_2$ and the formation of polyoxomolybdates.[22] However, the hydrolysis of $MoO_2(acac)_2$ was not complete, since a small band at 1540 cm^{-1} (C═O) and two bands at 1355 and 1278 cm^{-1} (C−C═C)[21,22] indicate the presence of acetylacetonate groups. For the Nafion film, typical absorption bands for C−F functionalities are found at 1218, 982, 635, and 511 cm^{-1}.[50] The band at 1060 cm^{-1} corresponds to the symmetric stretching vibration of the sulfonic group.[50] For the film obtained from the mixed solution, features of both Nafion and polyoxomolybdates are present. Nevertheless, the bands assigned to acetylacetonate group are not detected, probably due to the ligand exchange of the acetylacetonate group by sulfonic group that have stronger coordination with the polyoxomolybdates.

The complete hydrolysis of $MoO_2(acac)_2$ after mixing with Nafion is further confirmed by XPS measurements. Figure 3 shows the C 1s core-level spectra measured on films prepared from $MoO_2(acac)_2$, Nafion, and the mixed solutions, respectively. The C 1s of $MoO_2(acac)_2$ film shows two peaks that can be assigned to C═O bonds (286.8 eV) and C−C bonds (284.5 eV).[51] For the Nafion film, the C 1s spectra are well-fitted to three peaks, which may be attributed to CF_3 (294.4 eV), CF_2 (292 eV), and CF (288 eV).[52] However, for the film of the mixture, the peaks for C═O and C−C, assigned to acetylacetonate group, almost disappear. Very small peaks are observed, probably resulting from surface contamination. By comparing the O 1s core-level spectra of the different films (Figure 4), consistent results are obtained. The O 1s of $MoO_2(acac)_2$ film can be fitted to two peaks located at 531.9 eV (C═O) and 530.9 eV (Mo═O).[51,53] The O 1s of Nafion film can be deconvoluted into two peaks with binding energies at 535.3 and 532.7 eV, which are related to the oxygen in the sulfonic acid group and the oxygen in the ether configuration.[52] Nevertheless, the peak for C═O is not detected in the mixed film. Therefore, the C 1s and O 1s core-level spectra both indicate that the acetylacetonate group does not exist in the film spin coated from the mixed solution, which is consistent with the FT-IR results. From Mo 3d core-level spectra of the

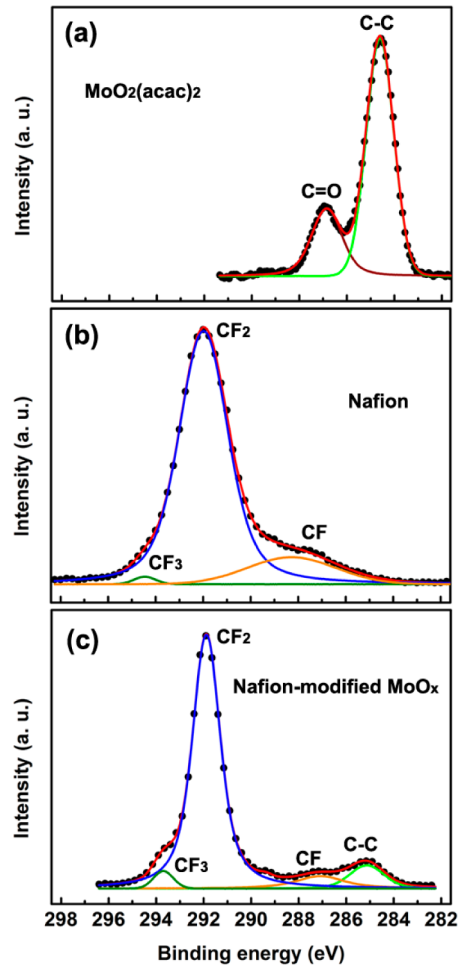

Figure 3. C 1s core-level spectra with the deconvoluted peaks of the films prepared from (a) $MoO_2(acac)_2$, (b) Nafion, and (c) the mixed solutions.

film obtained from $MoO_2(acac)_2$ solution (Figure 5a), two doublets can be found. The doublet located at 236.2 eV (Mo $3d_{5/2}$) and 233.1 eV (Mo $3d_{3/2}$) is related to Mo^{6+}, while the other doublet at lower binding energies implies the existence of a small portion of Mo^{5+}. The Mo 3d binding energies of Mo^{6+} measured here are similar to the values for MoO_3 and are higher than those for neat $MoO_2(acac)_2$,[53,54] which is another proof for the hydrolysis of $MoO_2(acac)_2$. In case of the film formed from the mixture solution, the peaks of Mo^{6+} shift slightly to higher binding energies (Figure 5b), probably due to the complete removal of acetylacetonate group and the coordination of sulfonic group. It is noteworthy to mention here that the neutralizer was turned on in some cases to neutralize the charged samples, which might also cause a minor shift of the energy scale. (charging was caused by the use of the relatively thick layers to obtain a high signal-to-noise ratio). Nevertheless, the broadening of the peaks observed in Figure 5b indicates the change of coordination environment of Mo^{6+}, which supports our assumption of the coordination of the sulfonic group.[55] Therefore, on the basis of both FT-IR and XPS measurements, we are able to conclude that the partial hydrolysis of $MoO_2(acac)_2$ first leads to the formation of polyoxomolybdates; by mixing them with Nafion, new complexes between polyoxomolybdate and Nafion are formed

DOI: 10.1021/am507459t
ACS Appl. Mater. Interfaces 2015, 7, 3581−3589

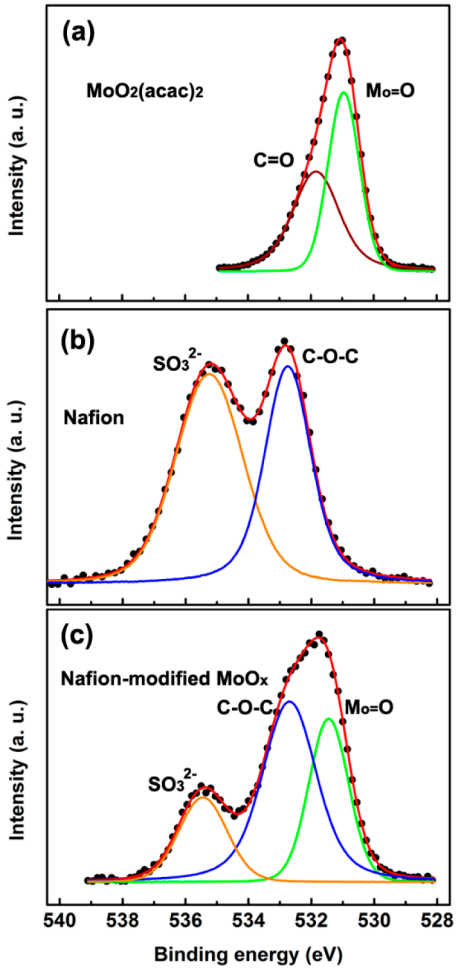

Figure 4. O 1s core-level spectra with the deconvoluted peaks of the films prepared from (a) $MoO_2(acac)_2$, (b) Nafion, and (c) the mixed solutions.

through the removal of acetylacetonate group and the coordination of the sulfonic group to polyoxomolybdate.

To demonstrate the effectiveness of our Nafion-modified MoO_x as HILs in organic solar cells, inverted P3HT:$PC_{60}BM$ devices (ITO/TiO_x/P3HT:$PC_{60}BM$/HILs/Ag) (Figure 6a) were fabricated and characterized. The performance of the Nafion-modified MoO_x HIL is compared to benchmark devices using evaporated MoO_3 or spin-coated PEDOT:PSS HILs. Unless mentioned, the concentration of $MoO_2(acac)_2$ is 0.4 mg/mL, while Nafion is diluted 50 times by 2-propanol and 1-butanol from its commercialized solution (see Experimental Section). The typical current density−voltage (J−V) and corresponding external quantum efficiency (EQE) curves of the devices using different HILs are shown in Figure 6b,c, respectively. The extracted device parameters of these devices are summarized in Table 1. It is necessary to note that the short circuit current density (J_{sc}) extracted from the device with evaporated MoO_3 is overestimated, probably due to the current collection from the outside of the defined active area. The Nafion-modified MoO_x-based device achieved J_{sc} of 9.65 mA/cm^2 (9.78 mA/cm^2 from EQE), open circuit voltage (V_{oc}) of 0.60 V, and fill factors (FF) of 60.3%, resulting in PCE of 3.49%. Such values are comparable to those obtained from the benchmark devices. Therefore, our Nafion-modified MoO_x HILs, prepared at room temperature, can work efficiently without any postdeposition treatments.

To achieve optimal performance in the previously described devices, the optimization of the $MoO_2(acac)_2$ concentration in the mixed solution is critical. In this study, we kept the concentration of Nafion constant (diluted by 50 times). The reason is that a too-high concentration of Nafion will dramatically increase the resistivity of the film, while a too-low concentration is harmful to the film formation on the active layers. Although a thin layer of Nafion has been introduced before to increase the work function of PEDOT:PSS,[56] pure Nafion cannot function as effective HIL for inverted devices. As shown in Figure 7, the deposition of a pure Nafion layer between the active layer and the Ag electrode leads to devices with very poor diode properties and extremely low V_{oc}, due to the bad contact at the anode side. By increasing the $MoO_2(acac)_2$ concentration, we observe three stages in the evolution of P3HT:$PC_{60}BM$ device performance. Such a phenomenon is reasonable considering that the thickness of our Nafion-modified MoO_x layer increases together with the $MoO_2(acac)_2$ concentration. For concentration lower than 0.4 mg/mL, all parameters improve with increasing $MoO_2(acac)_2$ concentration. At this stage, our HIL layer is either too thin or not able to fully cover the active layer, potentially resulting in direct contact of Ag with the active layer. For concentration higher than 2.4 mg/mL, the increased series resistance of the HILs degrades the FF of our devices (Figure 7c), while the V_{oc} remains unchanged (Figure 7b). When the $MoO_2(acac)_2$ concentration is in between the above-mentioned two values, the PCE of the P3HT:$PC_{60}BM$ devices remains constant, since the active layer is well protected from the Ag contact by our HIL and the resistances of the HIL are negligible. The above-mentioned evolution is also reflected in the change of dark

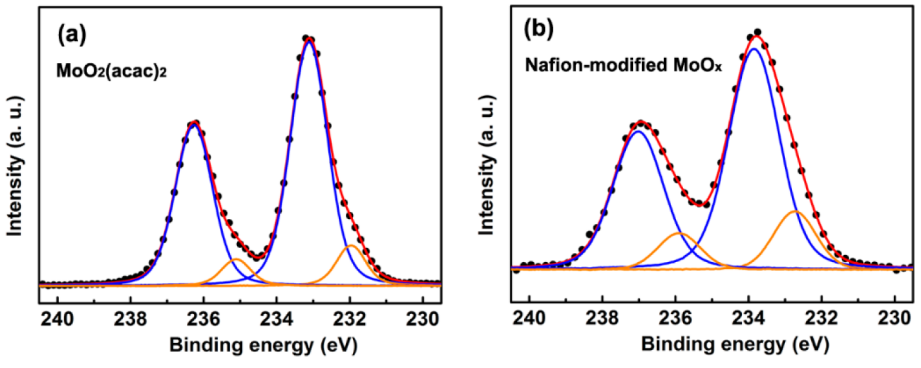

Figure 5. Mo 3d core-level spectra of the films obtained from (a) $MoO_2(acac)_2$ solution and (b) the mixed solution.

DOI: 10.1021/am507459t
ACS Appl. Mater. Interfaces 2015, 7, 3581−3589

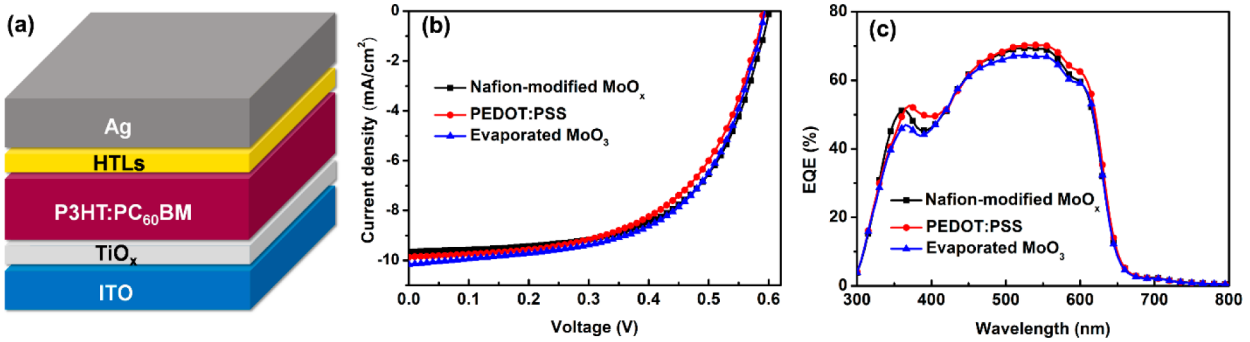

Figure 6. (a) Scheme of the P3HT:$PC_{60}BM$ device structure used in this study, (b) $J-V$ curves under illumination, and (c) EQE curves of P3HT:$PC_{60}BM$ devices based on different HILs.

Table 1. Detailed Photovoltaic Parameters of P3HT:$PC_{60}BM$ Device Using Different HILs, Extrapolated from the $J-V$ Curves

HILs	J_{sc}[a] (mA/cm^2)	V_{oc} (V)	FF (%)	PCE[a] (%)
Nafion-modified MoO_x	9.65 (9.78)	0.60	60.34	3.49 (3.54)
PEDOT:PSS	9.87 (10.01)	0.59	57.50	3.35 (3.37)
evaporated MoO_3	10.17 (9.58)	0.59	58.78	3.52 (3.32)

[a]The data shown in the brackets are the J_{sc} values calculated from the EQE curves in Figure 6c and the derived PCE values corresponding to the calculated J_{sc}, respectively.

curves of the devices (Figure 8). The device with pure Nafion has high leakage current density in reverse bias but low current density in forward bias, implying poor diode properties. The device fabricated with 0.1 mg/mL shows similar current density in forward bias compared to that of the device made with 0.4 mg/mL $MoO_2(acac)_2$, but the leakage current is a little higher. Conversely, the device with HIL fabricated from 2.4 mg/mL $MoO_2(acac)_2$ solution has similar leakage current to that of the

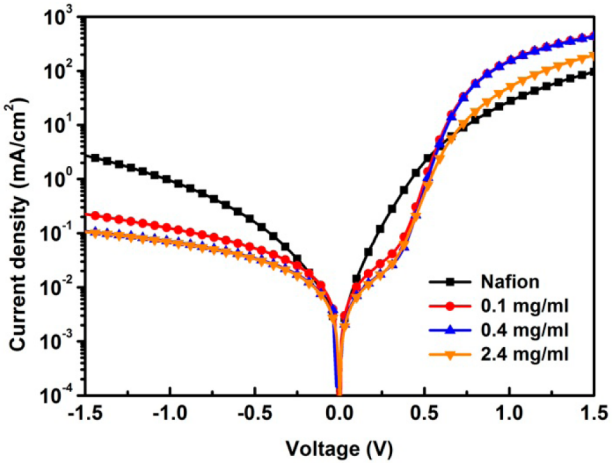

Figure 8. Dark curves of the P3HT:$PC_{60}BM$ devices using HILs made from pure Nafion, the mixed solution with 0.1, 0.4, and 2.4 mg/mL $MoO_2(acac)_2$, respectively.

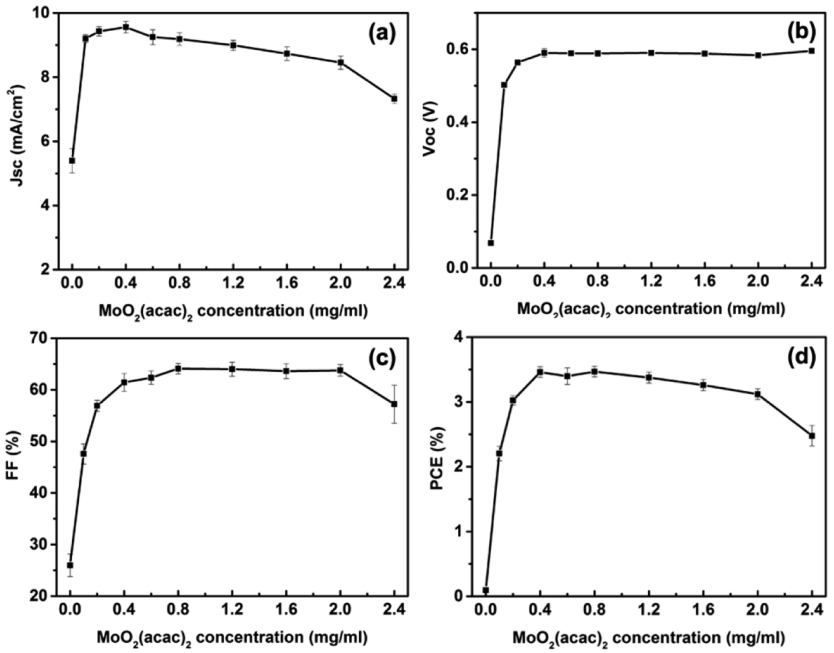

Figure 7. Evolution of J_{sc} (a), V_{oc} (b), FF (c), and PCE (d) of P3HT:$PC_{60}BM$ devices in function of $MoO_2(acac)_2$ concentration. The concentration of Nafion is constant, which is diluted 50 times by 2-propanol and 1-butanol. The zero point corresponds to pure Nafion. The error bars is the standard deviation of 12 devices.

DOI: 10.1021/am507459t
ACS Appl. Mater. Interfaces 2015, 7, 3581−3589

device made with 0.4 mg/mL $MoO_2(acac)_2$, but the current density in forward bias is much lower due to the high series resistance.

To verify the capability of our Nafion modified MoO_x for different types of active layers and for high efficiency organic solar cells, its performance in inverted devices, using the blend of a diketopyrrolopyrrole-based polymer material PDPP5T and $PC_{70}BM$ as active layer, was also evaluated. The chemical structure of PDPP5T is shown in Supporting Information, Figure S2. The detailed average photovoltaic parameters of the devices using our Nafion-modified MoO_x and evaporated MoO_3 are illustrated in Table 2, respectively. The corresponding EQE curves are also illustrated in Supporting Information, Figure S3. Clearly, the devices with the Nafion-modified MoO_3 HILs have almost identical efficiency with those using evaporated MoO_3 also in this material system, indicating its applicability for high-efficiency devices.

Table 2. Detailed photovoltaic parameters of PDPP5T:$PC_{70}BM$ devices using different HILs.

HILs	J_{sc}[a] (mA/cm^2)	V_{oc} (V)	FF (%)	PCE[a] (%)
Nafion-modified MoO_x	18.66 (18.63)	0.56	63.16	6.60 (6.59)
evaporated MoO_3	18.98 (17.81)	0.55	64.31	6.71 (6.30)

[a]The data shown in the brackets are the J_{sc} values calculated from the EQE curves in Supporting Information, Figure S3 and the derived PCE values corresponding to the calculated J_{sc}, respectively.

To complete the assessment of the properties of $MoO_2(acac)_2$, we also studied the impact of $MoO_2(acac)_2$ on the stability in organic solar cells in ambient air. The critical role of hole and electron transport layers in ambient air stability has been proven by numerous studies, making lifetime study of all novel transport layers imperative. Herein, using sol–gel TiO_x as electron injection layer, the air stability of P3HT:$PC_{60}BM$ inverted devices with our Nafion-modified MoO_x, PEDOT:PSS, and evaporated MoO_3 were compared. All the devices were stored in ambient air (~40%RH) in the dark, without encapsulation to accelerate the failure. The initial photovoltaic parameters are given in Supporting Information, Table S1, with the PCE of devices all above 3.5% for the three different HILs. The degradation trends of PCE, J_{sc}, V_{oc}, and FF over storage time are shown in Figure 9. The evolution of the PCE values follows two stages, independent of the nature of the HILs. During the first stage of air exposure, (below 1000 h), the PCE values slightly improved, because the FF increase compensates the loss in J_{sc} (Figure 9b,d). The improved device performance of inverted P3HT:$PC_{60}BM$ devices after air aging is in line with the results reported by another research group, suggesting that the improved hole extraction is due to the oxidation of Ag.[57] Meanwhile, the decreased dark current density at reverse bias is observed for all the devices

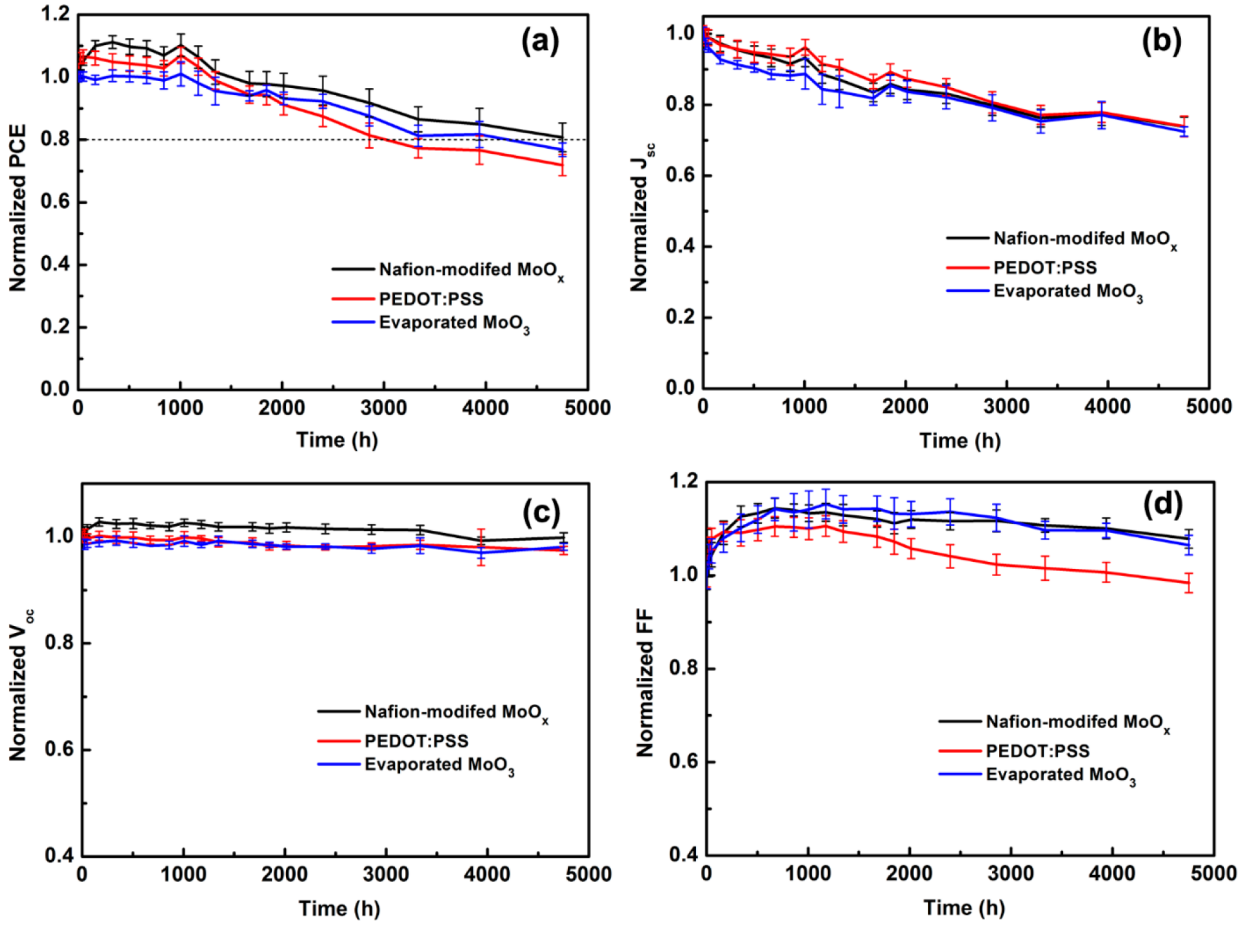

Figure 9. Degradation trends of the photovoltaic parameters over storage time for P3HT:$PC_{60}BM$ devices with different HILs. (a) Normalized PCE. (b) Normalized J_{sc}. (c) Normalized V_{oc}. (d) Normalized FF. The average and deviations are calculated from 12 devices. Devices were stored in ambient air without encapsulation.

DOI: 10.1021/am507459t
ACS Appl. Mater. Interfaces 2015, 7, 3581–3589

(Supporting Information, Figure S4), which may indicate improved contact selectivity and reduced interface recombination. It is noteworthy that device performance is measured upon light soaking of 5−15 min, with the duration increasing upon aging time, to reach the maximum PCE. Hence, we also inevitably thermally anneal the samples. The consequent slight morphology reorganization of P3HT:$PC_{60}BM$ blend may also lead to improved charge transport and reduced recombination and, hence, contribute to the improvement of the FF.[58,59] In the second stage of air aging, a faster degradation of FF in PEDOT:PSS devices is observed. By fitting the dark curves to the Shockley equation,[60] the evolution of series resistance for these three types of devices are shown in Figure 10. Though the

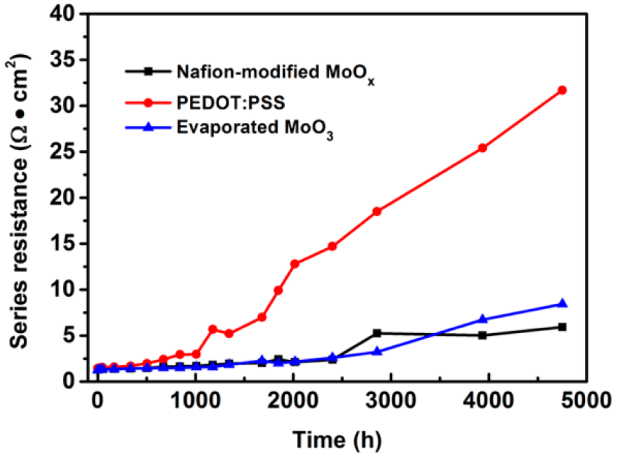

Figure 10. Evolution of series resistance over storage time for P3HT:$PC_{60}BM$ devices with different HILs.

initial series resistances are almost identical, it can be clearly observed that the series resistance of PEDOT:PSS devices became significantly higher than the Nafion-modified MoO_x and evaporated MoO_3 based devices after 1000 h of air aging, explaining the quicker decrease of FF. The increase of series resistance for PEDOT:PSS devices probably results from reduced conductivity of PEDOT:PSS after air exposure, as has been reported elsewhere.[15] The devices using our Nafion-modified MoO_x retain 80% of its initial PCE after the storage in air for 4752 h (so-called T80), which is longer than that for PEDOT:PSS (T80 = 2856 h) and for evaporated MoO_3 (T80 = 3336 h). This comparison demonstrates the superior stability of our Nafion-modified MoO_x compared to the two commonly used HILs.

3. CONCLUSIONS

In summary, room-temperature solution-processed hole injection layers for inverted organic photovoltaic devices are demonstrated using the combination of $MoO_2(acac)_2$ and Nafion. By using this mixture, complexes of polyoxomolybdates and Nafion are formed through ligand exchange reactions. Owing to the better interaction between the polymer backbone of Nafion and the hydrophobic active layer, smooth and continuous HILs are able to form on top of the active layers. Inverted devices with such Nafion-modified MoO_x hole injection layers have performance comparable to those with PEDOT:PSS or evaporated MoO_3. The device air stability with Nafion-modified MoO_x outperforms even its evaporated MoO_3 counterpart as it retains 80% of the initial PCE after 4752 h without encapsulation. Therefore, our solution-processed Nafion-modified MoO_x layer, compatible with large-scale solution-processing technologies, is a promising alternative to PEDOT:PSS for highly efficient and stable organic solar cells.

4. EXPERIMENTAL SECTION

4.1. Device Fabrication. $MoO_2(acac)_2$ and Nafion (5 wt % in lower aliphatic alcohols and water) were purchased from Sigma-Aldrich. $MoO_2(acac)_2$ was dissolved in mixed solvent of 2-propanol and 1-butanol (1:1 v/v) and stirred on a hot plate for 1 h at 60 °C to form a 20 mg/mL light yellow solution. This solution was stored at room temperature in a N_2 -filled glovebox. Nafion was diluted with a mixture of 2-propanol and 1-butanol. The Nafion-modified MoO_x solution was made by stirring the mixture of $MoO_2(acac)_2$ solution and the diluted Nafion for 20 min at room temperature before spin coating. The typical concentration of $MoO_2(acac)_2$ was 0.4 mg/mL, and the concentration of Nafion was kept at 0.1 wt % (diluted 50 times). The patterned ITO substrates were first cleaned with detergent and then ultrasonicated in deionized water, acetone, and 2-propanol for 10 min, respectively. After this, a sol−gel-prepared TiO_x solution was spin-coated on the cleaned ITO with a recipe reported previously.[61] For the P3HT:$PC_{60}BM$ devices, the *ortho*-dichlorobenzene solution of P3HT and $PC_{60}BM$ (1:0.8 weight ratio) was spin-coated on TiO_x to form the active layer with a thickness of 200 nm and then annealed at 130 °C for 10 min inside a nitrogen-filled glovebox. To fabricate the PDPP5T:$PC_{70}BM$ devices, the *ortho*-dichlorobenzene solution of PDPP5T and $PC_{70}BM$ (1:2 w/w) was spin-coated on TiO_x to form an 80 nm active layer. The Nafion-modified MoO_x HILs were then deposited on the active layers in a glovebox with a spin speed of 1000 rpm. For comparison, PEDOT:PSS or evaporated MoO_3 was also deposited on the active layers as the HIL. PEDOT:PSS was modified by 2-propanol and 1-butanol to get good wetting on P3HT:$PC_{60}BM$ layer. Finally, a 150 nm thick layer of Ag was evaporated through a shadow mask defining 12 devices (each of 0.13 cm^2 area) on one substrate.

4.2. Instruments and Device Characterization. Digital images were taken with an Olympus AX70 optical microscope in dark field mode. AFM images were recorded using aPicoscan PicoSPM LE scanning probe microscope in tapping mode. FT-IR spectra were obtained in transmission using a Bruker Vertex 70 FT-IR spectrometer equipped with a DTGS detector at a resolution of 4 cm^{-1}, and 32 scans were acquired in the spectral range of 4000−480 cm^{-1}. XPS experiments were performed on a Physical Electronics (PHI) 5600LS electron spectrometer, equipped with a small-spot X-ray source providing monochromatized Al Kα photons (1486.6 eV) with resolutions of <0.4 and 0.04 eV, respectively. The binding energy scale was calibrated by means of an independent Au reference sample, setting the Au 4f7/2 core-level position to 84.00 eV. Charged samples were neutralized by means of a Kimball Physics Inc. ELG-2 electron gun, using the C 1s core level (C−C bonds at 284.5 eV) as reference. The photovoltaic characteristics were measured under a nitrogen atmosphere using a Keithley 2602A Source-Measure Unit and an Abet solar simulator with 100 mW/cm^2 AM1.5G illumination, calibrated with an ISE Fraunhofer certified Si photodiode.

■ ASSOCIATED CONTENT

Supporting Information

The FT-IR spectra of $MoO_2(acac)_2$ powder measured using KBr pellet, the illustrated chemical structure of PDPP5T, EQE curves of PDPP5T:PC70BM devices, the initial average photovoltaic parameters of P3HT:$PC_{60}BM$ devices using different HILs for air stability test, the evolution of dark curves during air aging for P3HT:$PC_{60}BM$ devices based on different HILs. This material is available free of charge via the Internet at http://pubs.acs.org.

DOI: 10.1021/am507459t
ACS Appl. Mater. Interfaces 2015, 7, 3581−3589

AUTHOR INFORMATION

Corresponding Author

*E-mail: Weiming.Qiu@imec.be.

Notes

The authors declare no competing financial interest.

ACKNOWLEDGMENTS

This project has received funding from the European Union's Seventh Programme for research, technological development, and demonstration in the frame of ArteSun (Grant No. FP7-NMP-2013-SMALL-7/604397).

REFERENCES

(1) Brabec, C. J.; Gowrisanker, S.; Halls, J. J. M.; Laird, D.; Jia, S. J.; Williams, S. P. Polymer-Fullerene Bulk-Heterojunction Solar Cells. *Adv. Mater.* **2010**, *22*, 3839−3856.

(2) Dou, L.; You, J.; Hong, Z.; Xu, Z.; Li, G.; Street, R. A.; Yang, Y. 25th Anniversary Article: A Decade of Organic/Polymeric Photovoltaic Research. *Adv. Mater.* **2013**, *25*, 6642−6671.

(3) Heremans, P.; Cheyns, D.; Rand, B. P. Strategies for Increasing the Efficiency of Heterojunction Organic Solar Cells: Material Selection and Device Architecture. *Acc. Chem. Res.* **2009**, *42*, 1740−1747.

(4) Krebs, F. C.; Espinosa, N.; Hösel, M.; Søndergaard, R. R.; Jørgensen, M. 25th Anniversary Article: Rise to Power—OPV-Based Solar Parks. *Adv. Mater.* **2014**, *26*, 29−39.

(5) You, J. B.; Dou, L. T.; Yoshimura, K.; Kato, T.; Ohya, K.; Moriarty, T.; Emery, K.; Chen, C. C.; Gao, J.; Li, G.; Yang, Y. A Polymer Tandem Solar Cell with 10.6% Power Conversion Efficiency. *Nat. Commun.* **2013**, DOI: 10.1038/ncomms2411.

(6) Liu, Y.; Chen, C. C.; Hong, Z.; Gao, J.; Yang, Y. M.; Zhou, H.; Dou, L.; Li, G.; Yang, Y. Solution-Processed Small-Molecule Solar Cells: Breaking the 10% Power Conversion Efficiency. *Sci. Rep.* **2013**, *3*, 3356.

(7) Søndergaard, R.; Hösel, M.; D. Angmo, D.; Larsen-Olsen, T. T.; Krebs, F. C. Roll-to-Roll Fabrication of Polymer Solar Cells. *Mater. Today* **2012**, *15*, 36−49.

(8) Chen, S.; Manders, J. R.; Tsang, S. W.; So, F. Metal Oxides for Interface Engineering in Polymer Solar Cells. *J. Mater. Chem.* **2012**, *22*, 24202−24212.

(9) Hadipour, A.; Cheyns, D.; Heremans, P.; Rand, B. P. Electrode Considerations for the Optical Enhancement of Organic Bulk Heterojunction Solar Cells. *Adv. Energy Mater.* **2011**, *1*, 930−935.

(10) Yip, H. L.; Jen, A. K. Y. Recent Advances in Solution-Processed Interfacial Materials for Efficient and Stable Polymer Solar Cells. *Energy Environ. Sci.* **2012**, *5*, 5994−6011.

(11) Qiu, W. M.; Hadipour, A.; Muller, R.; Conings, B.; Boyen, H.; Heremans, P.; Froyen, L. Ultrathin Ammonium Heptamolybdate Films as Efficient Room-Temperature Hole Transport Layers for Organic Solar Cells. *ACS Appl. Mater. Interfaces* **2014**, *6*, 16335−16343.

(12) Voroshazi, E.; Verreet, B.; Buri, A.; Muller, R.; Di Nuzzo, D.; Heremans, P. Influence of Cathode Oxidation via the Hole Extraction Layer in Polymer:Fullerene Solar Cells. *Org. Electron.* **2011**, *12*, 736−744.

(13) Suh, Y.; Lu, N.; Lee, S. H.; Chung, W. S.; Kim, K.; Kim, B.; Ko, M. J.; Kim, M. J. Degradation of a Thin Ag Layer Induced by Poly(3,4ethylenedioxythiophene):Polystyrene Sulfonate in a Transmission Electron Microscopy Specimen of an Inverted Polymer Solar Cell. *Acs Appl. Mater. Interfaces* **2012**, *4*, 5118−5124.

(14) Norrman, K.; Madsen, M. V.; Gevorgyan, S. A.; Krebs, F. C. Degradation Patterns in Water and Oxygen of an Inverted Polymer Solar Cell. *J. Am. Chem. Soc.* **2010**, *132*, 16883−16892.

(15) Kawano, K.; Pacios, R.; Poplavskyy, D.; Nelson, J.; Bradley, D. D. C.; Durrant, J. R. Degradation of Organic Solar Cells Due to Air Exposure. *Sol. Energy Mater. Sol. Cells* **2006**, *90*, 3520−3530.

(16) Girotto, C.; Voroshazi, E.; Cheyns, D.; Heremans, P.; Rand, B. P. Solution-Processed MoO_3 Thin Films As a Hole-Injection Layer for Organic Solar Cells. *ACS Appl. Mater. Interfaces* **2011**, *3*, 3244−3247.

(17) Yang, T. B.; Wang, M.; Cao, Y.; Huang, F.; Huang, L.; Peng, J. B.; Gong, X.; Cheng, S. Z. D.; Cao, Y. Polymer Solar Cells with a Low-Temperature-Annealed Sol-Gel-Derived MoO_x Film as a Hole Extraction Layer. *Adv. Energy Mater.* **2012**, *2*, 523−527.

(18) Murase, S.; Yang, Y. Solution Processed MoO_3 Interfacial Layer for Organic Photovoltaics Prepared by a Facile Synthesis Method. *Adv. Mater.* **2012**, *24*, 2459−2462.

(19) Xie, F. X.; Choy, W. C. H.; Wang, C. D.; Li, X. C.; Zhang, S. Q.; Hou, J. H. Low-Temperature Solution-Processed Hydrogen Molybdenum and Vanadium Bronzes for an Efficient Hole-Transport Layer in Organic Electronics. *Adv. Mater.* **2013**, *25*, 2051−2055.

(20) Hammond, S. R.; Meyer, J.; Widjonarko, N. E.; Ndione, P. F.; Sigdel, A. K.; Garcia, A.; Miedaner, A.; Lloyd, M. T.; Kahn, A.; Ginley, D. S.; Berry, J. J.; Olson, D. C. Low-Temperature, Solution-Processed Molybdenum Oxide Hole-Collection Layer for Organic Photovoltaics. *J. Mater. Chem.* **2012**, *22*, 3249−3254.

(21) Tan, Z. A.; Qian, D. P.; Zhang, W. Q.; Li, L. J.; Ding, Y. Q.; Xu, Q.; Wang, F. Z.; Li, Y. F. Efficient and Stable Polymer Solar Cells with Solution-processed Molybdenum Oxide Interfacial Layer. *J. Mater. Chem. A* **2013**, *1*, 657−664.

(22) Jasieniak, J. J.; Seifter, J.; Jo, J.; Mates, T.; Heeger, A. J. A Solution-Processed MoO_x Anode Interlayer for Use within Organic Photovoltaic Devices. *Adv. Funct. Mater.* **2012**, *22*, 2594−2605.

(23) Chen, C. P.; Chen, Y. D.; Chuang, S. C. High-Performance and Highly Durable Inverted Organic Photovoltaics Embedding Solution-Processable Vanadium Oxides as an Interfacial Hole-Transporting Layer. *Adv. Mater.* **2011**, *23*, 3859−3863.

(24) Terán-Escobar, G.; Pampel, J.; Caicedo, J. M.; Lira-Cantú, M. Low-Temperature, Solution-Processed, Layered V_2O_5 Hydrate as the Hole-Transport Layer for Stable Organic Solar Cells. *Energy Environ. Sci.* **2013**, *6*, 3088−3098.

(25) Lee, S. J.; Pil Kim, H.; Mohd Yusoff, A. R.; Jang, J. Organic Photovoltaic with PEDOT:PSS and V_2O_5 Mixture as Hole Transport Layer. *Sol. Energy Mater. Sol. Cells* **2014**, *120*, 238−243.

(26) Kim, J.; Kim, H.; Kim, G.; Back, H.; Lee, K. Soluble Transition Metal Oxide/Polymeric Acid Composites for Efficient Hole-Transport Layers in Polymer Solar Cells. *ACS Appl. Mater. Interfaces* **2014**, *6*, 951−957.

(27) Zilberberg, K.; Trost, S.; Schmidt, H.; Riedl, T. Solution Processed Vanadium Pentoxide as Charge Extraction Layer for Organic Solar Cells. *Adv. Energy Mater.* **2011**, *1*, 377−381.

(28) Kim, J.; Yu, K.; Kim, H.; Kwon, S.; Kim, G.; Kwon, K.; Lee, K. Efficient Charge Extraction in Thick Bulk Heterojunction Solar Cells through Infiltrated Diffusion Doping. *Adv. Energy Mater.* **2014**, DOI: 10.1002/aenm.201301502.

(29) Zilberberg, K.; Trost, S.; Meyer, J.; Kahn, A.; Behrendt, A.; Lützenkirchen-Hecht, D.; Frahm, R.; Riedl, T. Inverted Organic Solar Cells with Sol−Gel Processed High Work-Function Vanadium Oxide Hole-Extraction Layers. *Adv. Funct. Mater.* **2011**, *21*, 4776−4783.

(30) Zhai, Z.; Huang, X.; Xu, M.; Yuan, J.; Peng, J.; Ma, W. Greatly Reduced Processing Temperature for a Solution-Processed NiO_x Buffer Layer in Polymer Solar Cells. *Adv. Energy Mater.* **2013**, *3*, 1614−1622.

(31) Bai, S.; Cao, M.; Jin, Y.; Dai, X.; Liang, X.; Ye, Z.; Li, M.; Cheng, J.; Xiao, X.; Wu, Z.; Xia, Z.; Sun, B.; Wang, E.; Mo, Y.; Gao, F.; Zhang, F. Low-Temperature Combustion-Synthesized Nickel Oxide Thin Films as Hole-Transport Interlayers for Solution-Processed Optoelectronic Devices. *Adv. Energy Mater.* **2014**, DOI: 10.1002/aenm.201301460.

(32) Steirer, K. X.; Ndione, P. F.; Widjonarko, N. E.; Lloyd, M. T.; Meyer, J.; Ratcliff, E. L.; Kahn, A.; Armstrong, N. R.; Curtis, C. J.; Ginley, D. S.; Berry, J. J.; Olson, D. C. Enhanced Efficiency in Plastic Solar Cells via Energy Matched Solution Processed NiO_x Interlayers. *Adv. Energy Mater.* **2011**, *1*, 813−820.

(33) Manders, J. R.; Tsang, S. W.; Hartel, M. J.; Lai, T. H.; Chen, S.; Amb, C. M.; Reynolds, J. R.; So, F. Solution-Processed Nickel Oxide

DOI: 10.1021/am507459t
ACS Appl. Mater. Interfaces 2015, 7, 3581−3589

Hole Transport Layers in High Efficiency Polymer Photovoltaic Cells. *Adv. Funct. Mater.* **2013**, *23*, 2993−3001.
(34) Stubhan, T.; Li, N.; Luechinger, N. A.; Halim, S. C.; Matt, G. J.; Brabec, C. J. High Fill Factor Polymer Solar Cells Incorporating a Low Temperature Solution Processed WO_3 Hole Extraction Layer. *Adv. Energy Mater.* **2012**, *2*, 1433−1438.
(35) Chen, L.; Xie, C.; Chen, Y. Optimization of the Power Conversion Efficiency of Room Temperature-Fabricated Polymer Solar Cells Utilizing Solution Processed Tungsten Oxide and Conjugated Polyelectrolyte as Electrode Interlayer. *Adv. Funct. Mater.* **2014**, 3986−3995.
(36) Tan, Z. A.; Li, L. J.; Cui, C. H.; Ding, Y. Q.; Xu, Q.; Li, S. S.; Qian, D. P.; Li, Y. F. Solution-Processed Tungsten Oxide as an Effective Anode Buffer Layer for High-Performance Polymer Solar Cells. *J. Phys. Chem. C* **2012**, *116*, 18626−18632.
(37) Li, N.; Stubhan, T.; Luechinger, N. A.; Halim, S. C.; Matt, G. J.; Ameri, T.; Brabec, C. J. Inverted Structure Organic Photovoltaic Devices Employing a Low Temperature Solution Processed WO_3 Anode Buffer Layer. *Org. Electron.* **2012**, *13*, 2479−2484.
(38) Zhu, Y.; Yuan, Z.; Cui, W.; Wu, Z.; Sun, Q.; Wang, S.; Kang, Z.; Sun, B. A Cost-Effective Commercial Soluble Oxide Cluster for Highly Efficient and Stable Organic Solar Cells. *J. Mater. Chem. A* **2014**, *2*, 1436−1442.
(39) Li, X.; Choy, W. C. H.; Xie, F.; Zhang, S.; Hou, J. Room-Temperature Solution-Processed Molybdenum Oxide as a Hole Transport Layer with Ag Nanoparticles for Highly Efficient Inverted Organic Solar Cells. *J. Mater. Chem. A* **2013**, *1*, 6614−6621.
(40) Han, D.; Yoo, S. The Stability of Normal vs. Inverted Organic Solar Cells under Highly Damp Conditions: Comparison with the Same Interfacial Layers. *Sol. Energy Mater. Sol. Cells* **2014**, *128*, 41−47.
(41) Sachs-Quintana, I. T.; Heumüller, T.; Mateker, W. R.; Orozco, D. E.; Cheacharoen, R.; Sweetnam, S.; Brabec, C. J.; McGehee, M. D. Electron Barrier Formation at the Organic-Back Contact Interface is the First Step in Thermal Degradation of Polymer Solar Cells. *Adv. Funct. Mater.* **2014**, 3978−3985.
(42) Lee, Y. J.; Yi, J.; Gao, G. F.; Koerner, H.; Park, K.; Wang, J.; Luo, K. Y.; Vaia, R. A.; Hsu, J. W. P. Low-Temperature Solution-Processed Molybdenum Oxide Nanoparticle Hole Transport Layers for Organic Photovoltaic Devices. *Adv. Energy Mater.* **2012**, *2*, 1193−1197.
(43) Meyer, J.; Khalandovsky, R.; Gorrn, P.; Kahn, A. MoO_3 Films Spin-coated from a Nanoparticle Suspension for Efficient Hole-injection in Organic Electronics. *Adv. Mater.* **2011**, *23*, 70−73.
(44) Sachs-Quintana, I. T.; Heumüller, T.; Mateker, W. R.; Orozco, D. E.; Cheacharoen, R.; Sweetnam, S.; Brabec, C. J.; McGehee, M. D. Electron Barrier Formation at the Organic-Back Contact Interface is the First Step in Thermal Degradation of Polymer Solar Cells. *Adv. Funct. Mater.* **2014**, 3978−3985.
(45) Gu, X.; Cui, W.; Li, H.; Wu, Z.; Zeng, Z.; Lee, S.-T.; Zhang, H.; Sun, B. A Solution-Processed Hole Extraction Layer Made from Ultrathin MoS_2 Nanosheets for Efficient Organic Solar Cells. *Adv. Energy Mater.* **2014**, *3*, 1262−1268.
(46) Yang, X.; Fu, W.; Liu, W.; Hong, J.; Cai, Y.; Jin, C.; Xu, M.; Wang, H.; Yang, D.; Chen, H. Engineering Crystalline Structures of Two-Dimensional MoS_2 Sheets for High-Performance Organic Solar Cells. *J. Mater. Chem. A* **2014**, *2*, 7727−7733.
(47) Zilberberg, K.; Gharbi, H.; Behrendt, A.; Trost, S.; Riedl, T. Low-temperature, Solution-Processed MoO_x for Efficient and Stable Organic Solar Cells. *ACS Appl. Mater. Interfaces* **2012**, *4*, 1164−1168.
(48) Knobler, C.; Penfold, B. R.; Robinson, W. T.; Wilkins, C. J.; Yong, S. H. Molybdenum(VI) Complexes From Diols and Amino-alchols: the Occurrence of MoO_2, Mo_2O_3, and Mo_2O_5 Core Structures. *J. Chem. Soc., Dalton Trans.* **1980**, 248−252.
(49) Ian Buckley, R.; Clark, R. J. H. Structural and Electronic Properties of Some Polymolybdates Reducible to Molybdenum blues. *Coord. Chem. Rev.* **1985**, *65*, 167−218.
(50) Ostrowska, J.; Narebska, A. Infrared Study of Hydration and Association of Functional Groups in a Perfluorinated Nafion Membrane, Part 1. *Colloid Polym. Sci.* **1983**, *261*, 93−98.
(51) Zhang, W.; Lin, S.; Wang, C.; Hu, J.; Li, C.; Zhuang, Z.; Zhou, Y.; Mathies, R. A.; Yang, C. J. PMMA/PDMS Valves and Pumps for Disposable Microfluidics. *Lab Chip* **2009**, *9*, 3088−3094.
(52) Schulze, M.; Lorenz, M.; Wagner, N.; Gülzow, E. XPS Analysis of the Degradation of Nafion. *Fresenius J. Anal. Chem.* **1999**, *365*, 106−113.
(53) Dupin, J. C.; Gonbeau, D.; Vinatier, P.; Levasseur, A. Systematic XPS Studies of Metal Oxides, Hydroxides and Peroxides. *Phys. Chem. Chem. Phys.* **2000**, *2*, 1319−1324.
(54) Grim, S. O.; Matienzo, L. J. X-Ray Photoelectron Spectroscopy of Inorganic and Organometallic Compounds of Molybdenum. *Inorg. Chem.* **1975**, *14*, 1014−1018.
(55) Spevack, P. A.; McIntyre, N. S. A Raman and XPS Investigation of Supported Molybdenum Oxide Thin Films. 1. Calcination and Reduction Studies. *J. Phys. Chem.* **1993**, *97*, 11020−11030.
(56) Esiner, S.; Eersel, H.; Wienk, M. M.; Janssen, R. A. Triple Junction Polymer Solar Cells for Photoelectrochemical Water Splitting. *Adv. Mater.* **2013**, *25*, 2932−2936.
(57) Lloyd, M. T.; Olson, D. C.; Lu, P.; Fang, E.; Moore, D. L.; White, M. S.; Reese, M. O.; Ginley, D. S.; Hsu, J. W. P. Impact of Contact Evolution on the Shelf Life of Organic Solar Cells. *J. Mater. Chem.* **2009**, *19*, 7638−7642.
(58) Liu, M. Y.; Chang, C. H.; Chang, C. H.; Tsai, K. H.; Huang, J. S.; Chou, C. Y.; Wang, I. J.; Wang, P. S.; Lee, C. Y.; Chao, C. H.; Yeh, C. L.; Wu, C. I.; Lin, C. F. Morphological Evolution of the Poly(3-Hexylthiophene)/[6,6]-Phenyl-C61-Butyric Acid Methyl Ester, Oxidation of the Silver Electrode, and Their Influences on the Performance of Inverted Polymer Solar Cells with a Sol−Gel Derived Zinc Oxide Electron Selective Layer. *Thin Solid Films* **2010**, *518*, 4964−4969.
(59) Irwin, M. D.; Buchholz, D. B.; Hains, A. W.; Chang, R. P. H.; Marks, T. J. p-Type Semiconducting Nickel Oxide as an Efficiency-Enhancing Anode Interfacial Layer in Polymer Bulk-Heterojunction Solar Cells. *Proc. Natl. Acad. Sci. U.S.A.* **2008**, *105*, 2783−2787.
(60) Rand, B. P.; Genoe, J.; Heremans, P.; Poortmans, J. Solar Cells Utilizing Small Molecular Weight Organic Semiconductors. *Prog. Photovoltaics* **2007**, *15*, 659−676.
(61) Hadipour, A.; Müller, R.; Heremans, P. Room Temperature Solution-Processed Electron Transport Layer for Organic Solar Cells. *Org. Electron.* **2013**, *14*, 2379−2386.

DOI: 10.1021/am507459t
ACS Appl. Mater. Interfaces 2015, 7, 3581−3589